The relationship between the interstitials location and visible light absorption in titanium dioxide: *ab initio* calculations

LEI LI[a,*], WENSHI LI[a], AIMIN JI[b], ZIOU WANG[a], CANYAN ZHU[b], LIJUN ZHANG[b], JIANFENG YANG[a], LING-FENG MAO[b,*]
[a]*Institute of Intelligent Structure and System, School of Electronics & Information Engineering, Soochow University, Suzhou 215006, P.R. China*
[b]*Institute of Intelligent Structure and System, Soochow University, Suzhou 215006, P.R. China*

The "*ab initio*" calculations about the impact of the different locations of Ti or Cu interstitials in TiO_2 on the visible light absorption are reported. We find the structure of TiO_2 with both the Ti and Cu interstitials in the different Ti columns produces the improved absorptions of the visible light than those in the lattice space or in the same Ti column. These differences attribute to the former structure induces the delocalized states in the shallow defect energy level below the Fermi energy level, while for the latter ones, the localized states in the deep defect energy levels above the valence band maximum.

1. Introduction

Since 1972, Titanium dioxide has attracted much attention in photocatalysis [1-5]. The transition-metal ions dopants into titanium dioxide are used to improve the visible-light absorption in the photocatalysts [6-9]. Choi et al. reported the doping with Fe^{3+}, Mo^{5+}, Ru^{3+}, Os^{3+}, Re^{5+}, V^{4+}, and Rh^{3+} increased the concentration of the trapped charge carriers, so enhanced the photodegradation of $CHCl_3$ under UV irradiation, while Co^{3+} and Al^{3+} dopants served as the recombination center so decreased photoactivity [10]. Zhang et. al. proved the Cr substituting Ti^{4+} ion in TiO_2 enhanced the photocatalytic activity of Cr-TiO_2 due to the excitation of 3d electron of the Cr^{3+} ion to the conduction band of TiO_2 [11]. Most researches have also been focused on Ti^{3+} self-doped TiO_2 which could exhibit better photocatalytic activity. Xing et. al. synthesized TiO_2 catalysts with self-doped Ti^{3+} and investigated their impact on the photocatalytic activity of visible-light and UV-light [12]. Zuo et. al. introduced Ti^{3+} into visible-light responsive TiO_2 to exhibit visible-light photocatalytic activity [13]. However, the photocatalytic activity on TiO_2 with the Ti^{3+} doping still face some problems, such as the relationship between the location of the Ti^{3+} doping and the photocatalytic activity of TiO_2. To resolve the issue, we introduce the Ti or Cu interstitials doping into the Ti column or the lattice space to study their impact on the visible light absorption.

2. Methods

We construct $2 \times 1 \times 6$ supercells (a = 9.188 Å, b = 4.594 Å, c = 17.754 Å) as the initial structure model on the primitive cell of the perfect TiO_2 (a = b = 4.594 Å, c = 2.959 Å). The Ti or Cu interstitials are doped in the same Ti-column in the $2 \times 1 \times 6$ supercells at (2.297, 2.297, 5.918) and (2.297, 2.297, 11.836), respectively. They are indicated in the blue balls marked with '2' and '1' of Fig. 1. These interstitials are also doped in the lattice space at (4.594, 2.297, 5.918) and (4.594, 2.297, 11.836), which are shown in the black balls marked with '4' and '3' of Fig. 1. They are doped in the different Ti-columns at (2.297, 2.297, 8.877) and (6.891, 2.297, 8.877), which are indicated in the green balls marked with '5' and '6' of Fig. 1. In the inset tables of Fig. 1, the '$Ti_{26}O_{48}$', '$Ti_{24}Cu_2O_{48}$', and '$Ti_{25}CuO_{48}$' mean the structure models include two Ti interstitials, two Cu interstitials, one Ti interstitials and one Cu interstitials, respectively. The '$ST-Ti_xO_y$', '$LS-Ti_xO_y$', and '$DT-Ti_xO_y$' mean the structure models with the interstitials in the same Ti-column (ST), in the lattice space (LS), and in the different Ti-columns (DT). In Figs. 2-4, the atoms pointed by the dark arrows belong to the Ti or Cu interstitials.

	1	2
ST-$Ti_{26}O_{48}$	Ti	Ti
ST-$Ti_{24}Cu_2O_{48}$	Cu	Cu
ST-$Ti_{25}CuO_{48}$	Ti	Cu

	3	4
LS-$Ti_{26}O_{48}$	Ti	Ti
LS-$Ti_{24}Cu_2O_{48}$	Cu	Cu
LS-$Ti_{25}CuO_{48}$	Ti	Cu

	5	6
DT-$Ti_{26}O_{48}$	Ti	Ti
DT-$Ti_{24}Cu_2O_{48}$	Cu	Cu
DT-$Ti_{25}CuO_{48}$	Ti	Cu

Ti   O
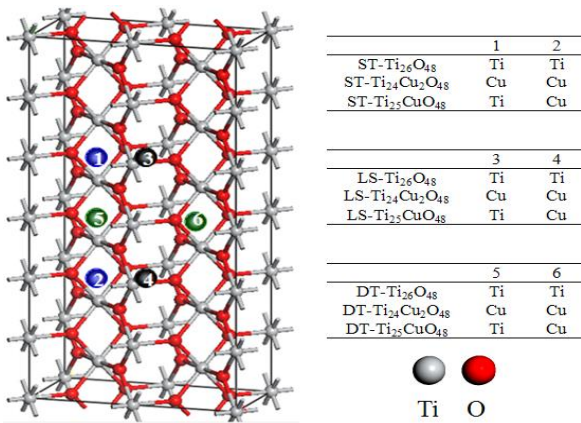
Fig. 1. Configuration of the TiO_2 with the Ti/Cu interstitials in the lattice space or in the Ti-columns.

The first-principles calculations are firstly performed by Dmol[3] program on the density functional theory [14]. Following the references of [15-18], we employ the PBE formulation (Perdew-Burke-Ernzerh) in the generalized gradient approximation (GGA) to discribe exchange-correlation energy [19]. The spin polarization method is applied to produce the semiconducting phenomenon for the transition metal oxides, such as of TiO_2. Double-numeric quality basis set with the polarization functions (DNP) is employed in the value of 3.5. The full Brillouin zone is defined with $3\times3\times2$ meshes of Monkhorst-Pack k points [20]. A thermal smearing of 0.01 Ha (1 Ha = 27.2114 eV) is used to accelerate the geometric optimization. The convergence tolerances for the self-consistent field (SCF) energy and displacement in the geometric optimization are set to 1.0×10^{-5} Ha and 5×10^{-3} Å. When the geometric optimization finished, the properties, such as band structure and partial density of states are calculated on Dmol[3] program. In the partial density of states, The curves with the light green color, the red color, and the blue color indicate the p states, the d states, and the sum states, respectively.

The absorption spetra and the electron density difference are calculated in CASTEP program [21]. The ultrasoft pseudopotentials are used to describe the electrons-ions interaction. The wave basis set with a cutoff energy of 400.0 eV is adopted. The k-points are set to $3\times3\times3$ meshes. In the electron density difference, the deficiencies of electrons are indicated in the yellow color, while the enrichment electrons in the blue color.

3. Results and discussion

Firstly, we would discuss the electron density difference to show the electron transfer in the structures with Ti or Cu interstitials. Figs. 2(a)-2(c) depict the isosurface of the electron density difference in DT-$Ti_{26}O_{48}$, DT-$Ti_{24}Cu_2O_{48}$, and DT-$Ti_{25}CuO_{48}$. The balls with the gray color, the red color, and the pink color indicate Ti-ions, O-ions, and Cu-ions, respectively. In Fig. 2(a), the belt liked electrons enrichment area in blue color locates between the lattice Ti-ions and the Ti interstitial. Thus, the Ti-Ti bonds are produced as the doping of the Ti interstitials. While, the Ti-Cu bonds are appeared after the Cu interstitials displacing for the Ti interstitials in Fig. 2(b). Moreover, some spots liked electrons deficiency areas in yellow color are found on the Cu interstitials. It means the Cu interstitials loss the electrons. In Fig. 2(c), both the Ti-Ti bond and the Ti-Cu bond are found.
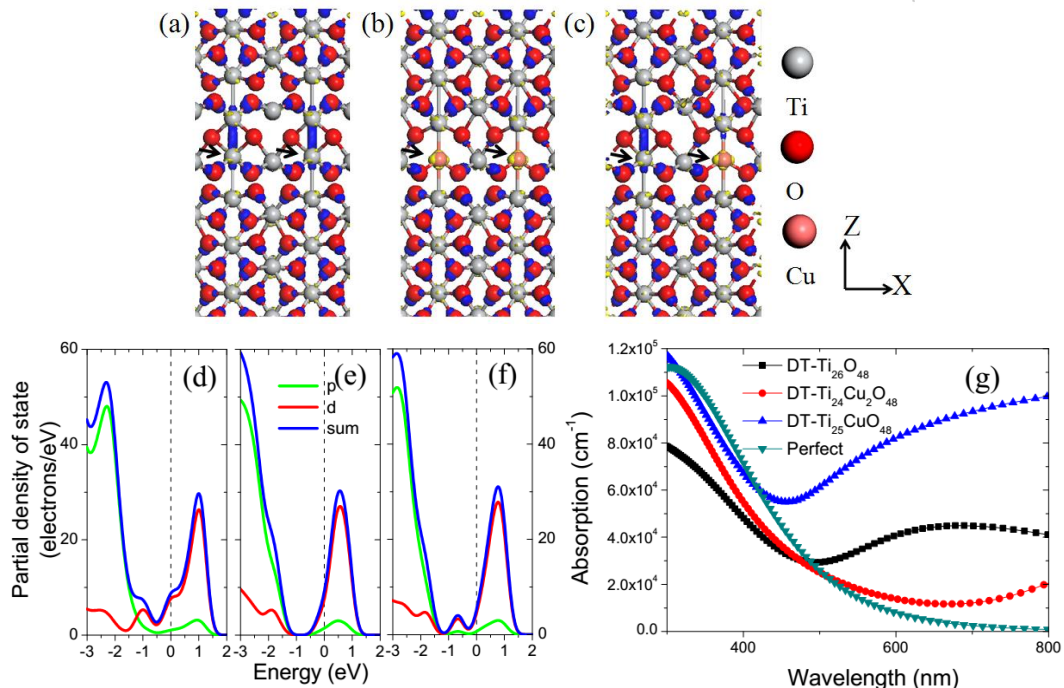
Fig. 2. (a-c) Isosurface of the electron density difference of the structures for DT-$Ti_{26}O_{48}$, DT-$Ti_{24}Cu_2O_{48}$, and DT-$Ti_{25}CuO_{48}$; (d-f) Partial density of states for DT-$Ti_{26}O_{48}$, DT-$Ti_{24}Cu_2O_{48}$, and DT-$Ti_{25}CuO_{48}$; (g) Absorption spectra of the above structures and perfect TiO_2.

Fig. 2(d)-2(f) show the partial density of states (PDOS) in DT-Ti$_{26}$O$_{48}$, DT-Ti$_{24}$Cu$_2$O$_{48}$, and DT-Ti$_{25}$CuO$_{48}$. In Fig. 2(d), it's clearly seen that one shallow defect energy level lies below the conduction band minimum (CBM) and one deep energy level above the valence band maximum (VBM). In Fig. 2(d), Fermi energy level locates at the shallow defect energy level. The doping of Ti interstitials generates the delocalized electrons, which are corresponding to the blue belt liked electron enrichments areas. The occurrence of the deep defect energy level above the VBM means the holes could be excided under the visible light. However, these holes could be recombined with the electrons. In Fig. 2(e), one defect energy level locates above the VBM. The fewer electrons would also be recombined with the holes. In Fig. 2(f), the defect energy level at -0.7 eV below the Fermi energy level would generate the delocalized electrons. So, these characteristics determine the order of visible light absorption at 500-800 nm is DT-Ti$_{25}$CuO$_{48}$ > DT-Ti$_{26}$O$_{48}$ > DT-Ti$_{24}$Cu$_2$O$_{48}$, as shown in Fig. 2(g).
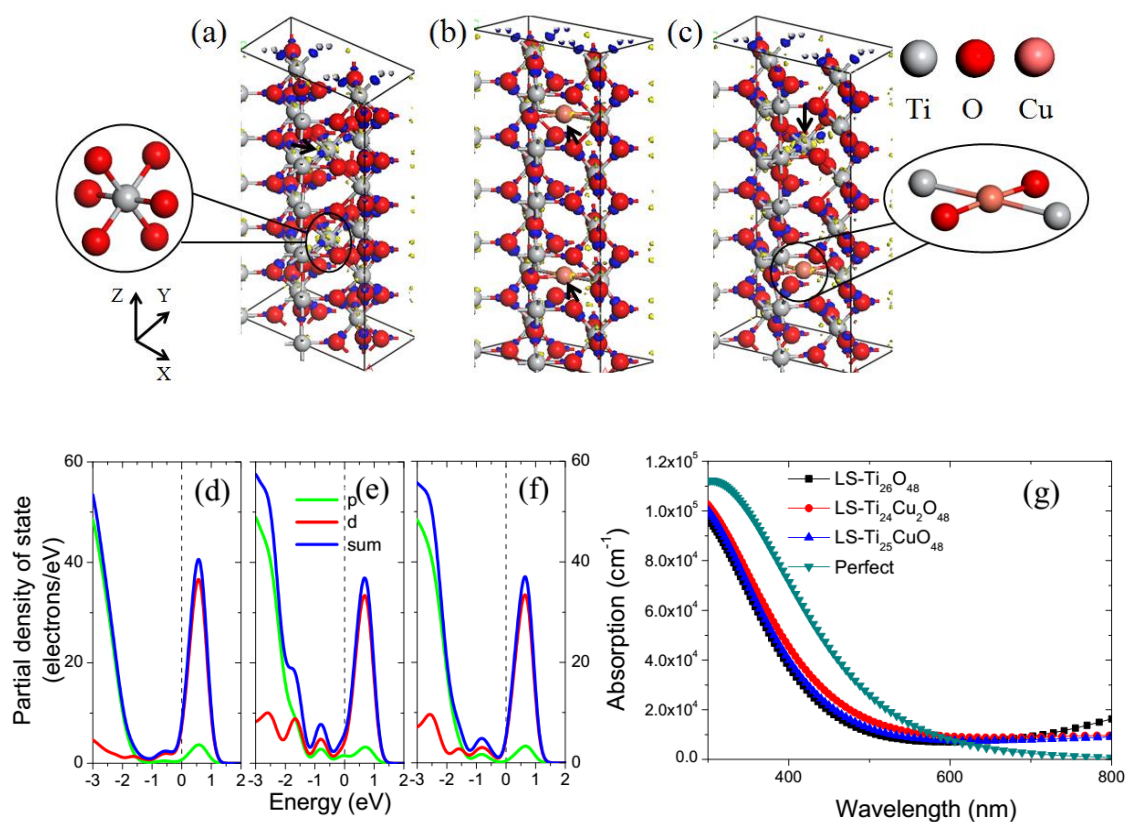
Fig. 3. (a-c) Isosurface of the electron density difference of the structures for LS-Ti$_{26}$O$_{48}$, LS-Ti$_{24}$Cu$_2$O$_{48}$, and LS-Ti$_{25}$CuO$_{48}$; (d-f) Partial density of states for LS-Ti$_{26}$O$_{48}$, LS-Ti$_{24}$Cu$_2$O$_{48}$, and LS-Ti$_{25}$CuO$_{48}$; (g) Absorption spectra of the above structures and perfect TiO$_2$.

For the structure of LS-Ti$_{26}$O$_{48}$, LS-Ti$_{24}$Cu$_2$O$_{48}$, and LS-Ti$_{25}$CuO$_{48}$, their electron density differences and partial density of states are shown in Fig. 3. In Figs. 3(a)-3(c), the Ti interstitials (1.29 eV) are bonding to six adjacent O-ions, while the Cu interstitials (0.58 eV) produce the Cu-O bonds and Ti-Cu bonds. In Fig. 3(d), the defect energy level locates below the CBM. It shows the delocalized electrons produced as the Ti interstitials in lattice space. In Fig. 3(e), one defect energy level lies above the VBM, and another one at -0.8 eV below the Fermi energy level. The recombination of electrons and holes are also happed in the structure of LS-Ti$_{24}$Cu$_2$O$_{48}$. In Fig. 3(f), in comparison with Fig. 3(e), the DOS of the defect energy levels are decreased. These aspects illustrate the higher absorption of visible light at 700-800 nm in LS-Ti$_{26}$O$_{48}$ than in other two structures.
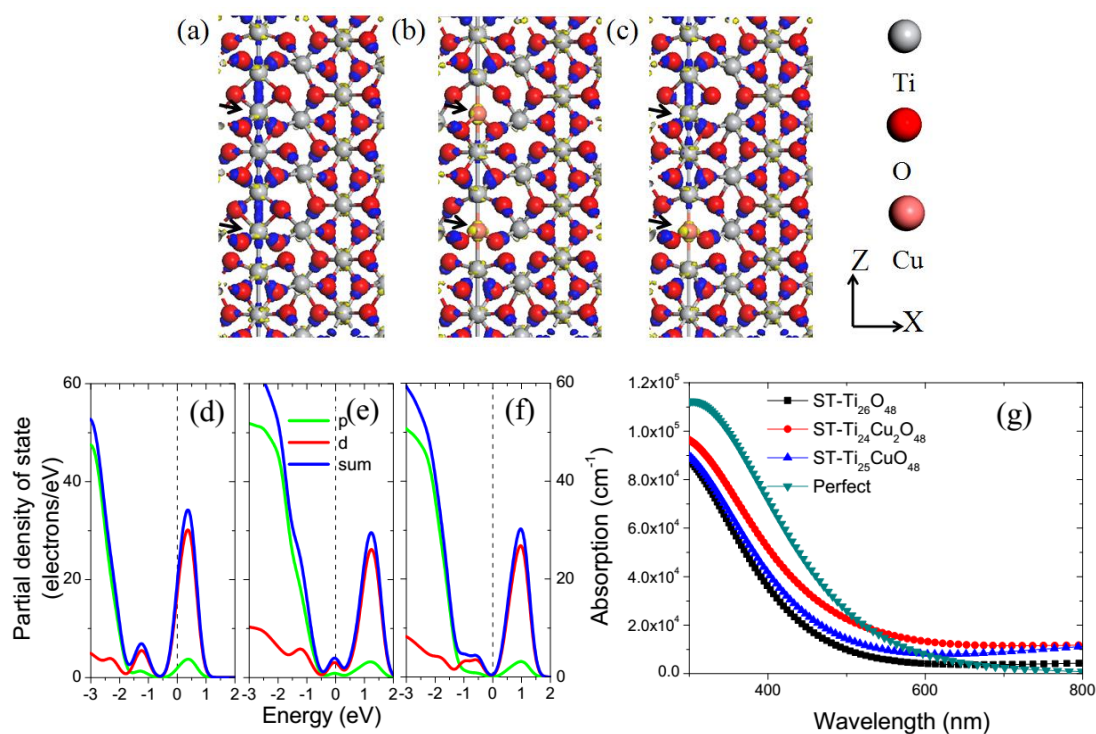
Fig. 4. (a-c) Isosurface of the electron density difference of the structures for ST-Ti$_{26}$O$_{48}$, ST-Ti$_{24}$Cu$_2$O$_{48}$, and ST-Ti$_{25}$CuO$_{48}$; (d-f) Partial density of states for ST-Ti$_{26}$O$_{48}$, ST-Ti$_{24}$Cu$_2$O$_{48}$, and ST-Ti$_{25}$CuO$_{48}$; (g) Absorption spectra of the above structures and perfect TiO$_2$.

Fig. 4 shows the electron density differences, partial density of states, and absorption spectra for the structure of ST-Ti$_{26}$O$_{48}$, ST-Ti$_{24}$Cu$_2$O$_{48}$, and ST-Ti$_{25}$CuO$_{48}$. In Figs. 4(a)-4(c), the Ti-Ti bonds and the Cu-Ti bonds are produced, which look like those in Fig. 2. In Fig. 4(d), the defect energy level locates at -1.3 eV below the Fermi energy. It shows the less delocalized electrons produced as the Ti interstitials in Ti-column. In Fig. 4(e), the defect energy level lies at 0 eV, where Fermi energy level locates. It means the more delocalized electrons produced than those in Fig. 4(d). The recombination of electrons and holes are also happed in the structure of ST-Ti$_{24}$Cu$_2$O$_{48}$. In Fig. 4(f), a serious of defect energy levels locates above the VBM. It shows that the recombination of electrons and holes are also happed in the structure of ST-Ti$_{25}$CuO$_{48}$, more extent than that in ST-Ti$_{24}$Cu$_2$O$_{48}$. These aspects illustrate the order of the absorption of visible light at 650-800 nm is ST-Ti$_{24}$Cu$_2$O$_{48}$ > ST-Ti$_{25}$CuO$_{48}$ > ST-Ti$_{26}$O$_{48}$.

4. Conclusions

We have compared the impact of the different location of Ti or Cu interstitials in TiO$_2$ on the visible light absorption in *ab initio* calculations. It's found that the absorptions of the visible light are improved in TiO$_2$ with both the Ti and Cu interstitials in the different Ti columns. It attributes to the delocalized states in the shallow defect energy level below the Fermi energy level. For TiO$_2$ with the interstitials in the lattice space and in the same Ti column, the less efficient absorptions of visible light are observed. It originates from the localized states in the deep defect energy levels above the valence band maximum.

References

[1] A. Fujishima, K. Honda, Nature **238**, 37 (1972).
[2] G. N. Schrauzer, T. D. Guth, J. Am. Chem. Soc. **99**, 7189 (1977).
[3] M. Halmann, Nature **275**, 115 (1978).
[4] T. Kawai, T. Sakata, Nature **286**, 474 (1980).
[5] J. Yu, Y. Su, B. Cheng, Adv. Funct. Mater. **17**, 1984 (2007).
[6] Z. S. Lin, A. Orlov, R. M. Lambert, M. C. Payne, J. Phys. Chem. B **109**, 20948 (2005).
[7] H. Xu, S. Ouyang, L. Liu, P. Reunchan, N. Umezawa, J. Ye, J. Mater. Chem. A **2**, 12642 (2014).

[8] R. Asahi, T. Morikawa, T. Ohwaki, K. Aoki, Y. Taga, Science **293**, 269 (2001).

[9] S. U. M. Khan, M. Al-Shahry, W. B. Jr. Ingler, Science **297**, 2243 (2002).

[10] W. Y. Choi, A. Termin, M. R. Hoffmann, J. Phys. Chem. **98**, 13669 (1994).

[11] J. F. Zhu, Z. G. Deng, F. Chen, J. L. Zhang, H. J. Chen, M. Anpo, J. Z. Huang, L. Z. Zhang, Appl. Catal. B Environ. **62**, 329 (2006).

[12] M. Xing, W. Fang, M. Nasir, Y. Ma, J. Zhang, M. Anpo, J. Catal. **297**, 236 (2013).

[13] F. Zuo, L. Wang, T. Wu, Z. Zhang, D. Borchardt, P. Feng, J. Am. Chem. Soc. **132**, 11856 (2010).

[14] L. Li, W. Li, A. Ji, Z. Wang, C. Zhu, L. Zhang, J. Yang, L. F. Mao, Phys. Chem. Chem. Phys. **17**, 17880 (2015).

[15] S. Livraghi, M. C. Paganini, E. Giamello, A. Selloni, C. D. Valentin , G. Pacchioni, J. Am. Chem. Soc. **15666**, 128 (2006).

[16] M. Harb, P. Sautet, P. Raybaud, J. Phys. Chem. C **115**, 19394 (2011).

[17] J. Tang, Z. Zou, J. Ye, J. Phys. Chem. C **111**, 12779 (2007).

[18] S. Meng, J. Ren, E. Kaxiras, Nano Lett. **8**, 3266 (2008).

[19] J. P. Perdew, K. Burke, M. Ernzerhof, M. Phys. Rev. Lett. **77**, 3865 (1996).

[20] H. J. Monkhorst, J. D. Pack, Phys. Rev. B **13**, 5188 (1976).

[21] M. D. Segall, P. L. D. Lindan, M. J. Probert, C. J. Pickard, P. J. Hasnip, S. J. Clarke, M. C. Payne, J. Phys.: Condens. Matter **14**, 2717 (2002).

_____

[*] Corresponding author: lei_li56@163.com

lingfengmao@suda.edu.cn